Simple and low-temperature synthesis of NiO nanoparticles through solid-state thermal decomposition of the hexa(ammine)Ni(II) nitrate, [Ni(NH$_3$)$_6$](NO$_3$)$_2$, complex

Saeid Farhadi *, Zeinab Roostaei-Zaniyani

Department of Chemistry, Lorestan University, Khoramabad 68135-465, Iran

ARTICLE INFO

ABSTRACT

NiO nanoparticles with an average size of about 12 nm were easily prepared *via* the thermal decomposition of hexa(ammine)Ni(II) nitrate complex, [Ni(NH$_3$)$_6$](NO$_3$)$_2$, at low temperature of 250 °C. The product was characterized by thermal analysis (TGA/DTA), X-ray diffraction (XRD), Fourier-transformed infrared spectroscopy (FT-IR), UV–Vis spectroscopy, BET specific surface area measurement, scanning electron microscopy (SEM), energy-dispersive X-ray spectroscopy (EDX), transmission electron microscopy (TEM), and magnetic measurement. The magnetic measurement revealed a small hysteresis loop at room temperature, confirming a superparamagnetic (weak ferromagnetic) nature of the synthesized NiO nanoparticles. Indeed, the NiO nanoparticles prepared by this method could be an appropriate semiconductor material due to the optical band gap of 3.35 eV which shows a red shift in comparison with the previous reports. This method is simple, fast, safe, low-cost and also suitable for industrial production of high purity NiO nanoparticles for applied purposes.

1. Introduction

Among transition metal oxides, nickel oxide (NiO) has been received considerable attention due to their wide range of applications in various fields, such as catalysis [1–3], electrochromic films [4–6], fuel cell electrodes [7] and gas sensors [8–10], battery cathodes [11–15] and magnetic materials [16–19], photovoltaic devices [20]. Furthermore, NiO is being studied for applications in smart windows [21], electrochemical supercapacitors [22] and dye-sensitized photocathodes [23]. Because of the quantum size and surface effects, NiO nanoparticles exhibit optical, catalytic, electronic, and magnetic properties that are significantly different than those of bulk-sized NiO particles [24,25]. For example, NiO nanostructures are p-type semiconductors with particular magnetic behaviors such as superparamagnetic, superantiferromagnetic, and ferromagnetic order depending on the particle size, particle shape, and synthesis route, whereas bulk-sized NiO is an antiferromagnetic insulator with a Neel temperature (T_N) of 250 °C [26,27].

Numerous new techniques have been developed for the preparation of NiO nanoparticle, such as ultrasonic radiation, pyrolysis by microwave, hydrothermal synthesis, sol–gel method, precipitation–calcination method, carbonyl method, laser chemical method, mechanochemical processing, microemulsion method, flame spray pyrolysis, solid-state method, and so forth [28–51]. Among them,

the method of solid-state thermal decomposition of complexes is one of the simplest and lowest-cost techniques for preparing pure transition metal oxides with relatively high specific surface area at low temperature [52–57]. This method not only avoided usage of the template and complex apparatus, but also exhibited affectivity in the shape control of the target product. By selecting a proper precursor, coupled with a rational calcining procedure, products with unique size and shapes could be obtained. This method also has potential advantages, including operational simplicity, high purity and high yield of product, no need for solvent, low energy consumption and no special equipment required.

In this work, we wish to report on the thermal decomposition of hexa(ammine)Ni(II) nitrate complex, [Ni(NH$_3$)$_6$](NO$_3$)$_2$, which resulted in the facile synthesis of pure NiO nanoparticles at low temperature of 250 °C. The product was identified by X-ray diffraction (XRD), Fourier-transformed infrared spectroscopy (FT-IR), UV–Vis spectroscopy, BET specific surface area measurement, scanning electron microscopy (SEM), energy-dispersive X-ray spectroscopy (EDX), transmission electron microscopy (TEM), thermal analysis (TG/DTA), and magnetic measurement.

2. Experimental

2.1. Preparation of [Ni(NH$_3$)$_6$](NO$_3$)$_2$ precursor

A solution of Ni(NO$_3$)$_2$·6H$_2$O (25 mmol) in 10 mL water was placed in an ice-water bath and treated with a slight stoichiometric excess (6 mL) of concentrated ammonia solution. The resultant

* Corresponding author. Tel.: +98 6612202782; fax: +98 6616200088.
E-mail address: sfarhad2001@yahoo.com (S. Farhadi).

violet crystals of $[Ni(NH_3)_6](NO_3)_2$ was completely precipitated by slow addition of 15 mL of cold ethanol. After standing for several hours in the cold, the crystals are filtered on a Buchner funnel, washed with alcohol, ether, and dried in open air at 50 °C. The complex was characterized by FT-IR, thermal analysis, and elemental analyses. *Anal.* Calc. for $[Ni(NH_3)_6](NO_3)_2$: Ni, 20.62; H, 6.32; N, 39.34. Found: Ni, 20.56; H, 6.41; N, 39.42.%.

2.2. Preparation of NiO nanoparticles

The $[Ni(NH_3)_6](NO_3)_2$ complex was decomposed at various temperatures for 1 h in ambient air. The temperatures for the decomposition of the complex in the range of 200–400 °C were selected from the results of TGA–DTA analysis. The decomposition products were collected for characterization.

2.3. Characterization techniques

The XRD patterns were recorded by a Rigaku D-max C III, X-ray diffractometer using Ni-filtered Cu Kα radiation (λ = 1.5406 Å) to determine the phases present in the decomposed samples. Infrared spectra were recorded on a Schimadzu system FT-IR 160 spectrophotometer using KBr pellets. The elemental analysis of the starting complex was performed using a Carlo Erba 1106 instrument. The thermal decomposition behavior of the precursor complex was studied by a Netzsch STA 409 PC/PG thermal analyzer at a heating rate of 10 °C/min in air. The optical absorption spectrum was recorded on a Shimadzu 1650PC UV–Vis spectrophotometer with the wavelength range of 300–700 nm at room temperature. The sample for UV–Vis studies was well dispersed in distilled water to form a homogeneous suspension by sonication for 25 min. The powder morphology was observed by a scanning electron microscope (SEM, Philips XL30) equipped with a link energy-dispersive X-ray (EDX) analyzer. The particle size was determined by a transmission electron microscope (TEM, Philips CM10) at an accelerating voltage of 80 kV. The powders were ultrasonicated in ethanol and a drop of the suspension was dried on a carbon-coated microgride for the TEM measurements. The magnetic properties of NiO nanoparticles were measured with a vibrating sample magnetometer (VSM) (BHV-55, Riken, Japan) at room temperature. The specific surface area of the product was measured by the BET method using N_2 adsorption–desorption isotherm carried out at −196 °C on a Surface Area Analyzer (Micromeritics ASAP 2010). Before each measurement, the sample was degassed at 150 °C for 2 h.

3. Results and discussion

Fig. 1 shows TG/DTA curves recorded for $[Ni(NH_3)_6](NO_3)_2$ at a constant heating rate of 10 °C min^{-1} in the temperature range of 25–600 °C. The TG curve shows that the decomposition of complex proceeds in three main stages. The first stage occurred at 155 °C, shows 12.25% weight-loss which is consistent with the theoretical value of 11.9% caused by the loss of two mole of NH_3 per mole of complex. On further heating to 180 °C in second stage, the residue complex shows about 12% weight-losses which related to liberate two other NH_3 ligands. In third stage, an extensive weight loss is observed at *ca.* 235 °C, followed by the gradual weight loss up to 250 °C. Above 250 °C, the weight remained constant, confirming the complete decomposition of the complex. The weight loss of all steps to be about 74% which is consistent with the theoretical value (73.76%) calculated for the formation of NiO from the complex. The DTA curve for the $[Ni(NH_3)_6](NO_3)_2$ complex as shown in the inset of Fig. 1, gave three characteristic peaks in consistent with TG data. The two small endothermic peaks at 155 and 180 °C can be explained by stepwise freeing four NH_3 molecules.
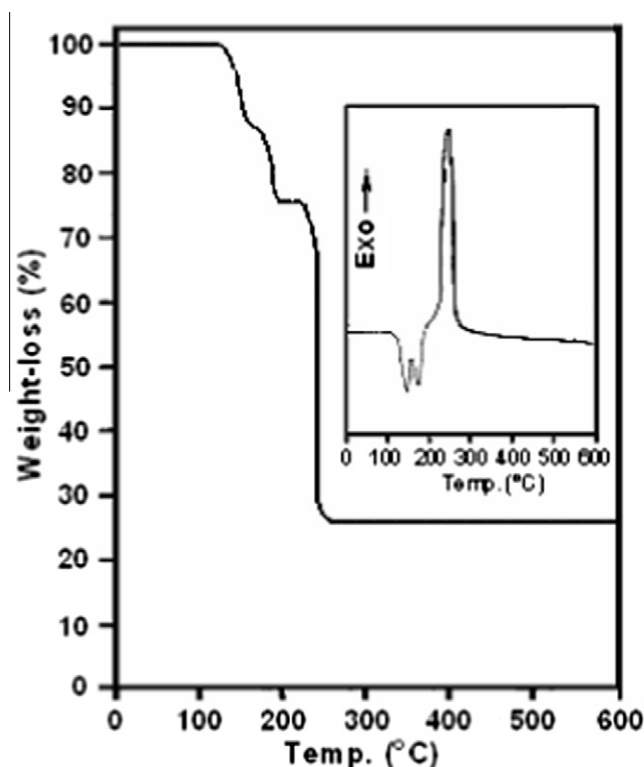
Fig. 1. TG and DTA (inset) curves of the $[Ni(NH_3)_6](NO_3)_2$ complex.

The de-ammination process resulted in the formation of the tetra- and diamine complexes, in succession, according to the following reactions:

$$[Ni(NH_3)_6](NO_3)_2 \rightarrow [Ni(NH_3)_4](NO_3)_2 + 2NH_3 \qquad \text{step 1} \qquad (1)$$

$$[Ni(NH_3)_4](NO_3)_2 \rightarrow [Ni(NH_3)_2](NO_3)_2 + 2NH_3 \qquad \text{step 2} \qquad (2)$$
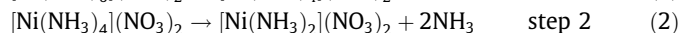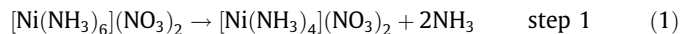
The composition of the $[Ni(NH_3)_2](NO_3)_2$ complex, the final product of the de-ammination process (steps 1 and 2), was confirmed by the elemental analysis, (*Anal.* Calc.: Ni, 27.11; H, 2.82; N, 25.93. Found: Ni, 27.09; H, 2.77; N, 25.84%) and the FT-IR spectrum (see Fig. 2b below). The endothermic de-ammination process is immediately followed by a big exothermic peak at about 235 °C. The sharp exothermic peak can be explained by the explosive decomposition of $[Ni(NH_3)_2](NO_3)_2$ complex *via* an intramolecular redox process taking place between the reductants (NH_3 ligands) and the oxidants (NO_3^-). The explosive redox reaction resulted in the solid NiO and gaseous products i.e. N_2, NO, N_2O and H_2O, according to the following reaction:

$$[Ni(NH_3)_2](NO_3)_2 \rightarrow NiO + (NO + N_2O + N_2) + H_2O \qquad \text{step 3}$$
$$(3)$$
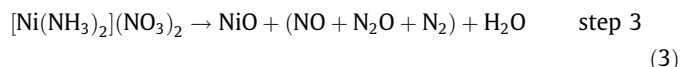
The FT-IR spectra of the complex samples decomposed at different temperatures are shown in Fig. 2. For the starting complex as shown in Fig. 2a, the characteristic stretching bands of NH_3 and NO_3 are observed at about 3250–3500 and 1350 cm^{-1}, respectively [58]. The intensity of these bands decreases when the complex is heated at 200 °C (Fig. 2b), so that the spectrum in this temperature can be related to the diamine $[Ni(NH_3)_2](NO_3)_2$ complex in consistent with the TG–DTA data described above. As can be seen in Fig. 2c, all bands of the complex were disappeared with increasing temperature to 250 °C and a strong band at around 440 cm^{-1} is observed which assigned to the Ni–O stretching of the octahedral NiO_6 groups in the face center cubic NiO structure [59]. At this temperature, the bands appeared at about 3550 and 1650 cm^{-1}
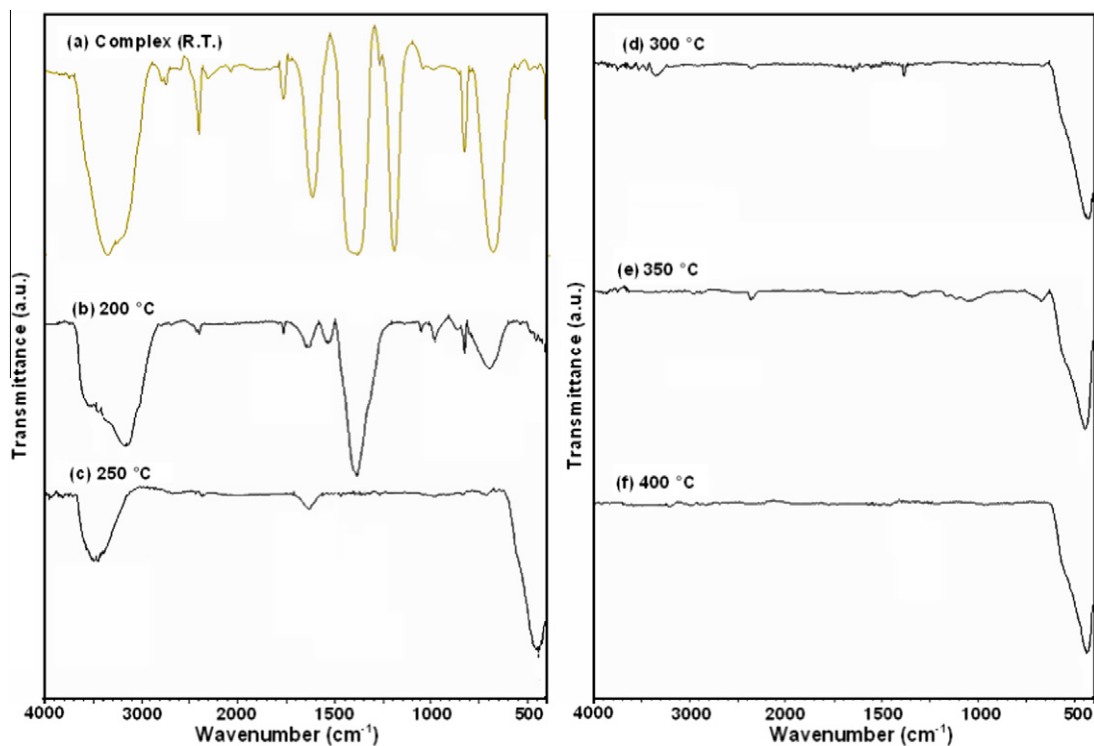
Fig. 2. FT-IR spectra of the $[Ni(NH_3)_6](NO_3)_2$ complex decomposed at various temperatures.

are related to the stretching and bending vibrations of the water molecules absorbed by the sample or KBr. As shown in Fig. 2b–f, in the FT-IR spectrum of the samples decomposed in the range of 300–400 °C, only the strong band related to the Ni–O stretching was observed without any change.

XRD patterns of the decomposition products of the $[Ni(NH_3)_6](NO_3)_2$ complex at various temperatures for 1 h are shown in Fig. 3. As shown in Fig. 3a, the XRD pattern of the sample decomposed at 250 °C reveals only the diffraction peaks attributable to NiO with face-centered cubic phase at $2\theta = 37.40°$, $43.45°$, $62.95°$, $75.40°$, and $79.45°$, which can be perfectly related to (1 1 1), (2 0 0), (2 2 0), (3 1 1), and (2 2 2) crystal planes, respectively (JCPDS Card No. 73-1523). This finding confirms that at 250 °C the complex was decomposed completely to nickel oxide. No peaks of impurity were found in the XRD pattern, indicating that the nanocrystalline NiO obtained *via* this synthesis method consists of ultrapure phase. It can be seen from Fig. 3a that the diffraction peaks are markedly broadened due to the small size effect of the particles. The average size of the NiO particles was estimated to be about 12.5 nm by the Debye–Scherrer equation [60]: $D_{XRD} = 0.9\lambda/(\beta cos\theta)$ where D_{XRD} is the average crystalline size, λ is the wavelength of Cu Kα, β is the full width at half maximum (FWHM) of the diffraction peak and θ is the Bragg's angle. As we can see in Fig. 3b and c, no new phase is observed when the decomposition temperature increases to 300, 350, and then 400 °C, but the width of the NiO peaks decreases with an increase in the decomposition temperature because of crystallite growth.

Fig. 4 shows the SEM images of $[Ni(NH_3)_6](NO_3)_2$ complex and its decomposition product at 250 °C. The SEM micrographs of the starting complex at two different scales are presented in Fig. 4a and b. It is obvious that the starting complex powder was made of very large needle crystals in different sizes. The SEM images of the product in Fig. 4c and d clearly shows that the shape and size of particles are quite different from that of the precursor complex. It can be seen that the product was formed from extremely fine semi-spherical particles which were loosely aggregated. No char-

acteristic morphology of the complex is observed, indicating the complete decomposition into the extremely fine spherical particles.

Fig. 5 shows the TEM image of the NiO product. The TEM sample was prepared with the dispersion of powder in ethanol by ultrasonic vibration. As shown in Fig. 5, the uniform NiO particles have sphere shapes with weak agglomeration. The particle sizes possess a narrow distribution in a range from 8 to 16 nm, and the mean particle diameter is about 12 nm. Actually, the mean particle size determined by TEM is very close to the average particle size calculated by Debye–Scherer formula from the XRD pattern.

Fig. 6 shows the EDX analysis of the product. Ni and O signals come from the NiO nanoparticles and the atomic percentages of Ni and O are 50.44% and 49.56%, respectively. Furthermore, the ratio of Ni and O is about 1:0.98 consistent with the theoretical value of NiO. The Si and Au signals come from the coating material of the instrument.

BET surface area measurements were also made on the NiO nanoparticles obtained from the decomposition of complex at 250 °C. The specific surface area of the product was 73.75 m^2/g. Assuming the NiO nanoparticles are almost spherical, as confirmed by TEM, the surface area can be used to estimate the particle size according to $D_{BET} = 6000/(\rho \times S_{BET})$ equation, where D_{BET} is the diameter of a spherical particle (in nm), ρ is the theoretical density of NiO (6.67 g/cm^3), and S_{BET} is the specific surface area of NiO powder in m^2/g. The particle size calculated from the surface area data is about 12.25 nm, which is in good agreement with the XRD and TEM results.

As shown in Fig. 7, the optical properties of the NiO nanoparticles were investigated by UV–Vis spectroscopy. In order to a comparison, UV–Vis spectra of the starting $[Ni(NH_3)_6](NO_3)_2$ complex and a commercial bulk NiO powder in water solvent were also presented in Fig. 7. As expected, the aqueous solution of the starting complex in Fig. 7a shows two weak d–d bands at about 385 and 665 nm (the third band shielded by CT band) while only a strong band at 335 nm is observed on the UV–Vis spectrum of the NiO
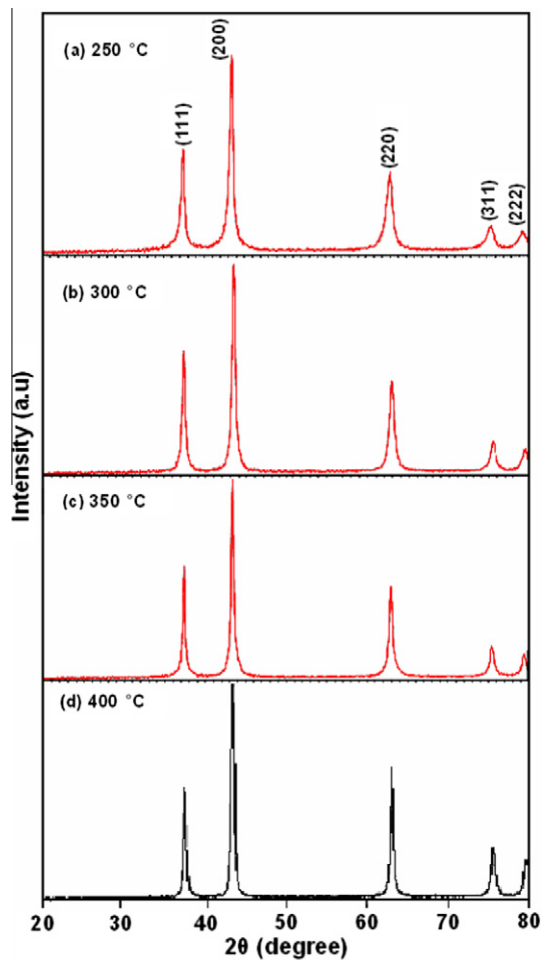
Fig. 3. XRD patterns of the $[Ni(NH_3)_6](NO_3)_2$ complex decomposed at selected temperatures.
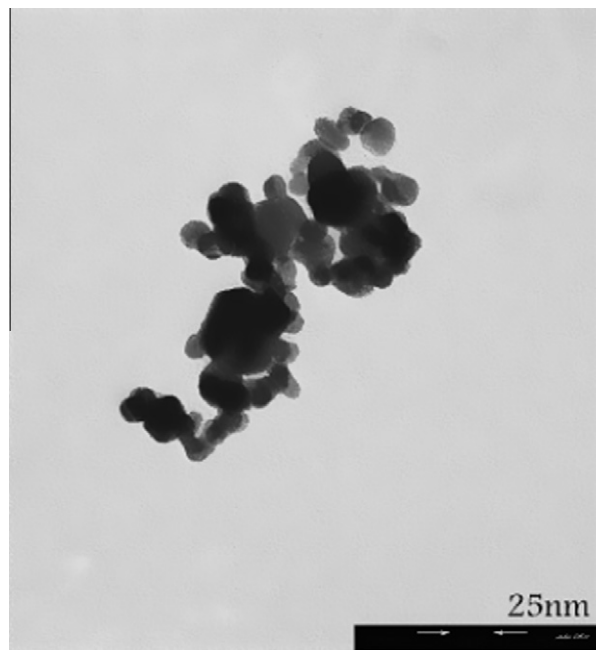
Fig. 5. TEM image of the NiO nanoparticles.

nanoparticles in Fig. 7b. It is clearly evident that UV–Vis spectrum of the NiO nanoparticles is quit different from that of the starting complex, confirming that the strong band appeared at 335 nm is due to NiO nanoparticle not Ni^{2+}. In addition, the UV–Vis spectrum of a commercial bulk NiO powder (Fig. 7c) does not show any observable absorption band, further confirming that the strong band appeared at 335 nm is characteristic of the NiO nanoparticles. Thus, the NiO nanoparticles prepared by this method could be a promising photocatalytic material. The strong absorption band is attributed to the electronic transition from the valence band to
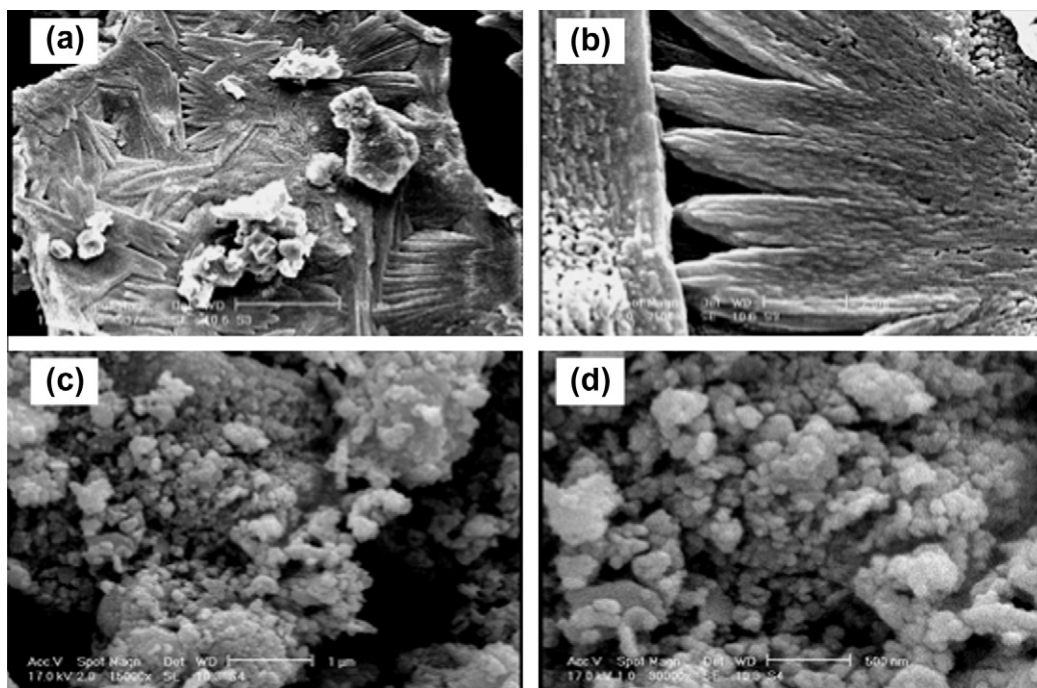
Fig. 4. SEM micrographs of the $[Ni(NH_3)_6](NO_3)_2$ complex (a and b) and the NiO nanoparticles (c and d) at different scales.
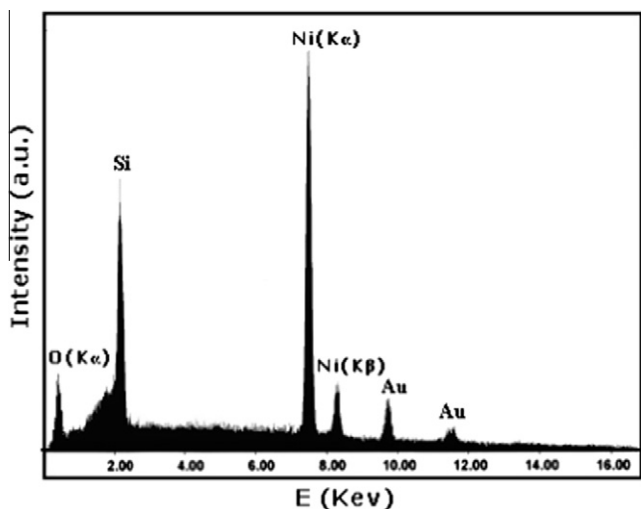
Fig. 6. EDX spectrum of the NiO nanoparticles.

the conduction band in the NiO semiconductor [53–56]. The direct optical band gap (E_g) of NiO nanoparticles can be calculated by the $(Ah\nu)^2 = B(h\nu - E_g)$ equation, where $h\nu$ is the photon energy, A is the absorption coefficient, B is a constant relative to the material.

The inset of Fig. 7 shows the plot of $(Ah\nu)^2$ versus $h\nu$ for the NiO sample. By the extrapolation on the linear region of this curve, the band gap was estimated to be about 3.35 eV, which shows some red shift in comparison with the previous reports [61,62].

The room temperature magnetic behavior of the NiO nanoparticles presented in Fig. 8a and b shows a small hysteresis loop. As shown in Fig. 8b, the shape of the hysteresis loop is characteristic of superparamagnetic (weak ferromagnetic) behavior although bulk NiO is antiferromagnetic [53–55,62–67]. From Fig. 8b, the coercive field (H_c) and the remanent magnetization (M_r) are estimated to be only 66 Oe and 0.002 emu/g. The maximum field applied, 7 kOe does not saturate the magnetization and the magnetization at this applied field is 0.065 emu/g. The low coercive field and remanent magnetization confirm that NiO nanoparticles exhibit a little ferromagnetic property. The non-saturation of the magnetization is characteristic of superparamagnetic (weak ferromagnetic) ordering of the spins in the nanoparticles. Nickel oxide nanoparticles are made of small magnetic domains. Each magnetic domain is characterized by its own magnetic moment oriented randomly. The total magnetic moment of the nanoparticles is the sum of these magnetic domains coupled by dipolar interactions [63]. As a result, a low value of M_s is obtained. The magnetic properties of nanomaterials have been believed to be highly dependent on the sample shape, crystallinity, magnetization direction, and so on.
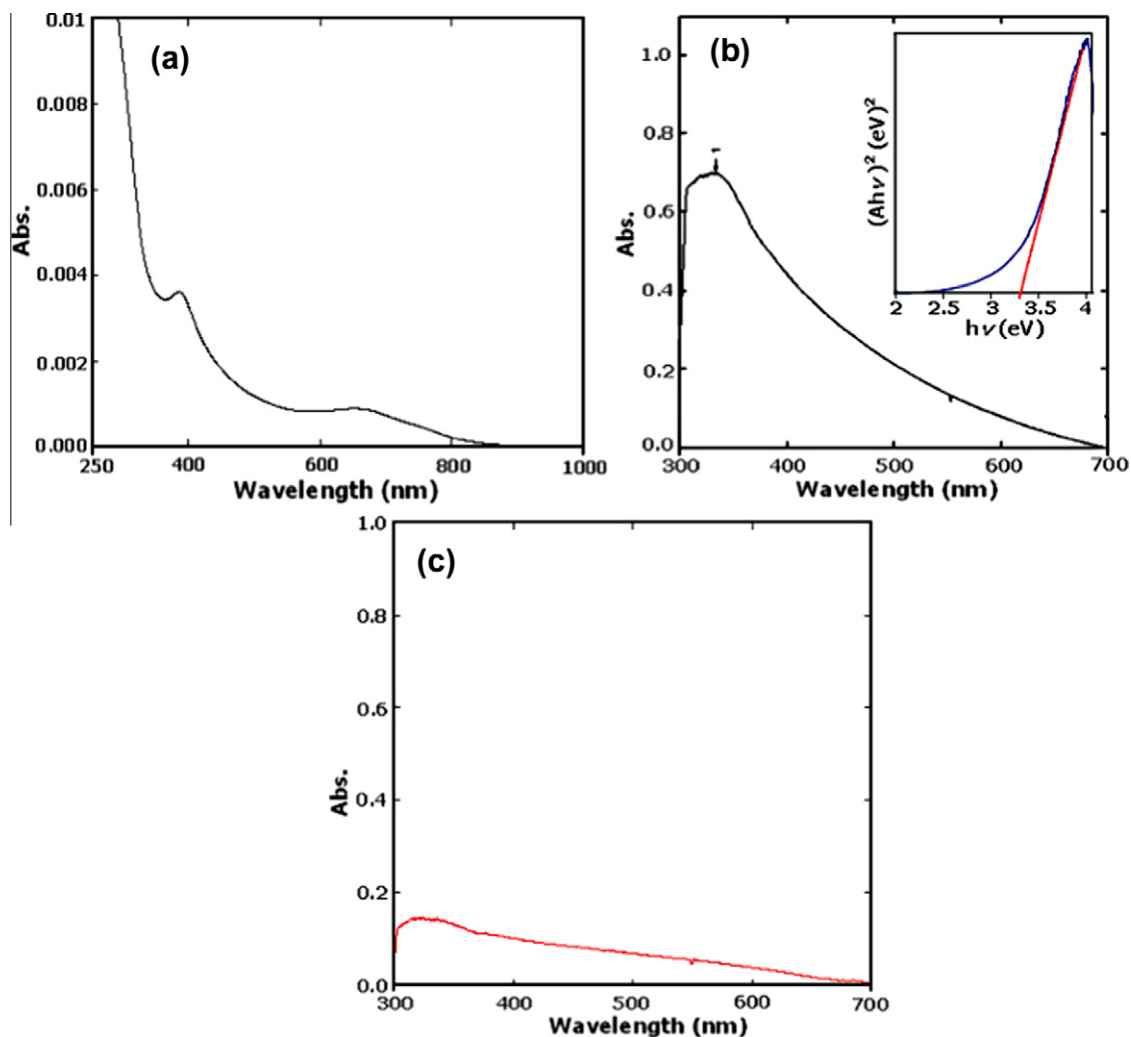
Fig. 7. (a) UV–Vis spectrum of aqueous solution of the $[Ni(NH_3)_6](NO_3)_2$ complex, (b) UV–Vis spectrum and $(Ah\nu)^2 - h\nu$ curve (inset) of the NiO nanoparticles, and (c) UV–Vis spectrum of a commercial bulk NiO powder.
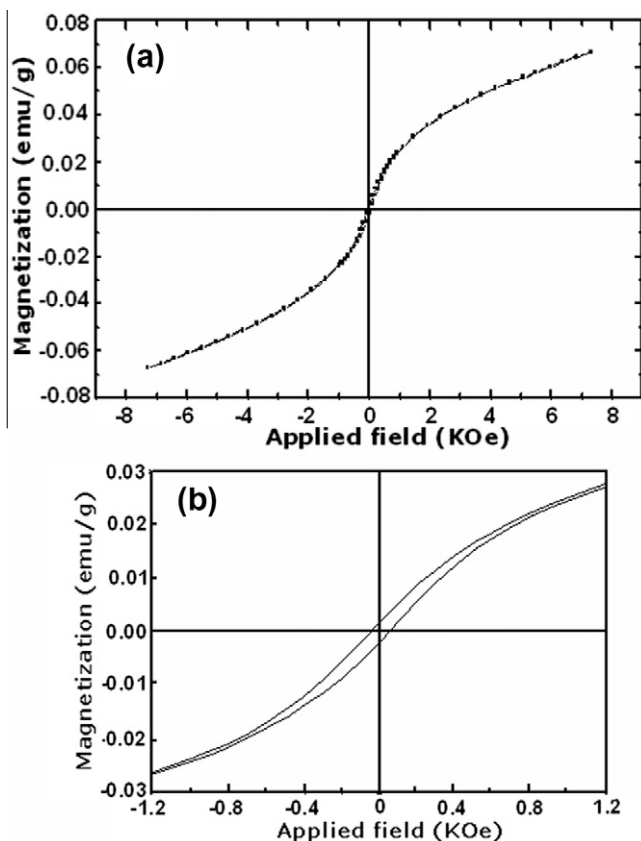
Fig. 8. (a) Magnetization versus applied magnetic field at room temperature for the NiO nanoparticles. (b) Enlarged view of the hysteresis loop in the low-field region.

4. Conclusions

In summary, pure and nanosized NiO particles with an average particle size of 13 nm were successfully synthesized through thermal decomposition of the $[Ni(NH_3)_6](NO_3)_2$ complex as a precursor at 250 °C. From this complex, NiO is formed *via* the de-ammination process and then explosive decomposition of residue $[Ni(NH_3)_2]$-$(NO_3)_2$ complex due to redox process taking place between the reductants (NH_3 ligands) and the oxidants (NO_3^-). By this method, uniform and spherical NiO nanoparticles with weak agglomeration, narrow size distribution and superparamagnetic (weak ferromagnetic) behavior can be obtained. The optical absorption band gap of the NiO nanoparticles is 3.35 eV. This method is simple, low-cost, safe and suitable for industrial production of high purity NiO nanoparticles for various applications. The synthetic route can be further used for the synthesis of other transition metal oxides.

References

[1] W. Wei, X. Jiang, L. Lu, X. Yang, X. Wang, J. Hazard. Mater. 168 (2009) 838.
[2] Nagi R.E. Radwan, M.S. El-Shall, Hassan M.A. Hassan, Appl. Catal. A: Gen. 331 (2007) 8.
[3] N.M. Deraz, M.M. Selim, M. Ramadan, Mater. Chem. Phys. 113 (2009) 269.
[4] Y. Ichiyanagi, N. Wakabayashi, J. Yamazaki, Physica B 329–333 (2003) 862.
[5] J.L. Garcia-Miquel, Q. Zhang, S.J. Allen, A. Rougier, A. Blyr, H.O. Davies, Thin Solid Films 424 (2003) 165.
[6] W.Y. Li, L.N. Xu, J. Chen, Adv. Funct. Mater. 15 (2005) 851.
[7] F. Li, H.Y. Chen, C.M. Wang, K.S. Hu, J. Electroanal. Chem. 531 (2002) 53.
[8] I. Hotovy, J. Huran, L. Spiess, S. Hascik, V. Rehacek, Sens. Actuators B: Chem. 57 (1999) 147.
[9] E.L. Miller, R.E. Rocheleau, J. Electrochem. Soc. 144 (1997) 3072.
[10] H.X. Yang, Q.F. Dong, X.H. Hu, J. Power Sources 79 (1999) 256.
[11] F.B. Zhang, Y.K. Zhou, H.L. Li, Mater. Chem. Phys. 83 (2004) 260.
[12] I. Hotový, J. Huran, L. Spiess, Vacuum 58 (2000) 300.
[13] X.H. Huang, J.P. Tu, B. Zhang, C.Q. Zhang, Y. Li, Y.F. Yuan, H.M. Wu, J. Power Sources 161 (2006) 541.
[14] D. Leevin, J.Y. Ying, Stud. Surf. Sci. Catal. 110 (1997) 367.
[15] M. Yoshio, Y. Todorov, K. Yamato, J. Power Sources 74 (1998) 46.
[16] Y. Wu, G. Wu, X. Ni, J. Vac. Sci. Technol. 19 (1999) 228.
[17] M. Ghosh, K. Biswas, A. Sundaresan, C.N.R. Rao, J. Mater. Chem. 16 (2006) 106.
[18] S.A. Makhlouf, F.T. Parker, F.E. Spada, A.E. Berkowitz, J. Appl. Phys. 81 (1997) 5561.
[19] T. Ahmad, K.V. Ramanujachary, S.E. Lofland, A.K. Ganguli, Solid State Sci. 8 (2006) 425.
[20] M. Borgstrom, E. Blart, G. Boschloo, E. Mukhtar, A. Hagfeldt, L. Hammarstrom, J. Phys. Chem. B 109 (2005) 22928.
[21] C.G. Granqvist (Ed.), Handbook of Inorganic Electrochromic Materials, Elsevier, Amsterdam, 1995.
[22] T. Nathan, A. Aziz, A.F. Noor, S.R.S. Prabaharan, J. Solid State Electrochem. 12 (2008) 1003.
[23] J. He, H. Lindström, A. Hagfeldt, S.E. Lindquist, J. Phys. Chem. B 103 (1999) 8940.
[24] G. Schmidt, Nanoparticles: From Theory to Application, VCH, Weinheim, 2004.
[25] E.T. Goldvurt, B. Kulkarni, R.N. Bhargava, J. Lumin. 72 (1997) 190.
[26] S.A. Makhlouf, F.T. Parker, F.F. Spada, A.F. Berkowitz, J. Appl. Phys. 81 (1997) 5561.
[27] Y. Ichiyanagi, N. Wakabayashi, J. Yamazaki, S. Yamada, Y. Kimishima, E. Komatsu, H. Tajima, Physica B 329 (2003) 862.
[28] X.Y. Deng, Z. Chen, Mater. Lett. 58 (2004) 276.
[29] V.R.R. Pulimi, P. Jeevanandam, J. Magn. Magn. Mater. 321 (2009) 2556.
[30] S.F. Wang, L.Y. Shi, X. Feng, Sh.R. Ma, Mater. Lett. 61 (2007) 1549.
[31] D.Y. Han, H.Y. Yang, C.B. Shen, X. Zhou, F.H. Wang, Powder Tech. 147 (2004) 113.
[32] P. Palanisamy, A.M. Raichur, Mater. Sci. Eng. C 29 (2009) 199.
[33] D.V. Lysov, D.V. Kuznetsov, A.G. Yudin, D.S. Muratov, V.V. Levina, D.I. Ryzhonkov, Nanotechnol. Russia 5 (2010) 493.
[34] E.R. Beach, K. Shqau, S.E. Brown, S.J. Rozeveld, P.A. Morris, Mater. Chem. Phys. 115 (2009) 371.
[35] E. Beach, S. Brown, K. Shqau, M. Mottern, Z. Warchol, P. Morris, Mater. Lett. 62 (2008) 1957.
[36] Z. Wei, H. Qiao, H. Yang, C. Zhang, X. Yan, J. Alloys Compd. 479 (2009) 855.
[37] T.L. Lai, Y.Y. Shub, G.L. Huangb, C.C. Lee, C.B. Wang, J. Alloys Compd. 450 (2008) 318.
[38] A. Surca, B. Orel, B. Pihlar, P. Bukovec, J. Electroanal. Chem. 408 (1996) 83.
[39] Y. Wu, Y. He, T. Wu, T. Chen, W. Weng, H. Wan, Mater. Lett. 61 (2007) 3174.
[40] S. Thota, J. Kumar, J. Phys. Chem. Solids 68 (2007) 1951.
[41] W.N. Wang, Y. Itoh, I.W. Lenggoro, K. Okuyama, Mater. Sci. Eng. B 111 (2004) 69.
[42] I.W. Lenggoroa, Y. Itoh, N. Iid, K. Okuyama, Mater. Res. Bull. 38 (2003) 1819.
[43] N. Dharmaraj, P. Prabu, S. Nagarajan, C.H. Kim, J.H. Park, H.Y. Kim, Mater. Sci. Eng. B 128 (2006) 111.
[44] X. Chen, Z. Zhang, C. Shi, X. Li, Mater. Lett. 62 (2008) 346.
[45] D. Tao, F. Wei, Mater. Lett. 58 (2004) 3226.
[46] Z. Chen, A. Xu, Y. Zhang, N. Gu, Curr. Appl. Phys. 10 (2010) 967.
[47] L. Jian-fen, X. Bo, D. Li-juan, Y. Rong, L.T. David, J. Fuel. Chem. Technol. 36 (2008) 42.
[48] C. Xu, K. Hong, S. Liua, G. Wang, X. Zhao, J. Cryst. Growth 255 (2003) 308.
[49] E.A. Souza, J.G.S. Duque, L. Kubota, C.T. Meneses, J. Phys. Chem. Solids 68 (2007) 594.
[50] X. Ni, Q. Zhao, F. Zhou, H. Zheng, J. Cheng, B. Li, J. Cryst. Growth 289 (2006) 299.
[51] Q. Li, L.S. Wang, B.Y. Hu, C. Yang, L. Zhou, L. Zhang, Mater. Lett. 61 (2007) 1615.
[52] E. Traversa, M. Sakamoto, Y. Sadaoka, Part. Sci. Technol. 16 (1998) 185.
[53] M. Salavati-Niasari, F. Mohandes, F. Davar, M. Mazaheri, M. Monemzadeh, N. Yavarinia, Inorg. Chim. Acta 362 (2009) 3691.
[54] F. Davar, Z. Fereshteh, M. Salavati-Niasari, J. Alloys Compd. 476 (2009) 797.
[55] M. Salavati-Niasari, N. Mir, F. Davar, Polyhedron 28 (2009) 1111.
[56] X. Li, X. Zhang, Z. Li, Y. Qian, Solid State Commun. 137 (2006) 581.
[57] S. Farhadi, N. Rashidi, Polyhedron 503 (2010) 439.
[58] K. Nakamoto, Infrared and Raman Spectra of Inorganic and Coordination Compounds, Part B: Applications in Coordination, Organometallic, and Bioinorganic Chemistry, sixth ed., Wiley, New York, 2009.
[59] C. Wang, C. Shao, L. Wang, L. Zhang, X. Li, Y. Liu, J. Colloid Interface Sci. 333 (2009) 242.
[60] H.P. Klug, L.E. Alexander, X-ray Diffraction Procedures, second ed., Wiley, New York, 1964.
[61] G. Boschloo, A. Hagfeldt, J. Phys. Chem. B. 195 (2001) 3039.
[62] A.T. Ngo, P. Bonville, M.P. Pileni, Eur. Phys. J.B 9 (1999) 583.
[63] M. Salavati-Niasari, Z. Fereshteh, F. Davar, Polyhedron 28 (2009) 1065.
[64] F. Mohandes, F. Davar, M. Salavati-Niasari, J. Magn. Magn. Mater. 322 (2010) 872.
[65] M. Salavati-Niasar, F. Davar, Z. Fereshteh, J. Alloys Compd. 476 (2009).
[66] M. Salavati-Niasar, F. Davar, Z. Fereshteh, J. Alloys Compd. 494 (2010) 410.
[67] A.S. Bhatt, D.K. Bhat, C.-W. Tai, M.S. Santosh, Mater. Chem. Phys. 125 (2011) 347.